Eleventh South African Conference on Computational and Applied Mechanics
SACAM 2018
Vanderbijlpark, South Africa, 17-19 September 2018

Adaptive SAFE model of a rail for parameter estimation

Isaac I. Setshedi[a,b,*], Craig S. Long[b], Philip W. Loveday[b], Daniel N. Wilke[a]

[a]*University of Pretoria, Lynnwood Road Hatfield, Pretoria, 0002, South Africa*

[b]*CSIR Material Science and Manufacturing, Meiring Naude Road Brummeria, Pretoria, 0184, South Africa*

email address : u10319965@tuks.co.za[a,b], clong@csir.co.za[b], ploveday@csir.co.za[b], nico.wilke@up.ac.za[a]

Abstract

Permanently installed monitoring systems, which make use of guided wave ultrasound, can monitor long distances of rail track from a single transducer location. The design of these systems is complicated by the presence of numerous modes of propagation and dispersion. The dispersion characteristics are used during signal processing and need to be known accurately. The semi-analytical finite element (SAFE) method has become a popular method for efficiently computing dispersion curves of elastic waveguides. The dispersion curves of a rail are dependent on material properties as well as the rail geometry, neither of which are known to a sufficient degree of accuracy. The rail geometry in particular changes over time due to wear and regular maintenance operations which include rail grinding of the crown. It would therefore useful if the dispersion curves of the rail or rail properties can be estimated from measured signals obtained by the monitoring system.

In this paper the forward problem of using a SAFE model with minimal input parameters to accurately compute dispersion characteristics is investigated. Three modes of propagation that are known to propagate long distances were analyzed and a method for tracking these mode shapes was developed. The mesh convergence with different elements was computed and a Q8 element was found to be the most efficient. Reduction of size of the eigenvalue problem by using Guyan reduction was demonstrated.

Three geometric parameters of the rail head were found to be sufficient to describe a range of possible rail geometries produced by rail grinding and wear. A technique for automatically adapting the mesh of the rail cross-section for the different geometric parameters, based on radial basis functions, was implemented. It was shown that the elastic modulus, density and frequency can be combined into one parameter and that the solutions to the eigenvalue problem solved for a range of this parameter may be scaled to produce dispersion curves as a function of frequency for different elastic moduli and densities. The eigenvalue problem has to be solved again for a range of this parameter if the Poisson's ratio is changed.

The efficient SAFE model with minimal input parameters presented will reduce the computation required when the inverse problem of estimating rail parameters from measured dispersion characteristics is investigated in future.

Keywords: SAFE, rail, mesh adaptation, material and geometry parameterisation, Guyan reduction

1. Introduction

Guided wave ultrasound (GWU) is very attractive for non-destructive evaluation and monitoring of elongated structures such as pipes and rails. Propagating waves can be excited using permanently installed piezoelectric transducers, and can propagate long distance (kilometres in some cases) [1]. A guided wave ultrasound based monitoring system has been developed and is currently being used to monitor approximately 840km of the Sishen-Saldanha ore export line [1]. The installed system works in pitch-catch mode, with alternating transmit and receive stations, and detects only complete rail breaks. Current research is aimed at upgrading the system to detect reflections from cracks before a complete break occurs, and employs a pulse-echo mode of operation as illustrated in Fig. 1.

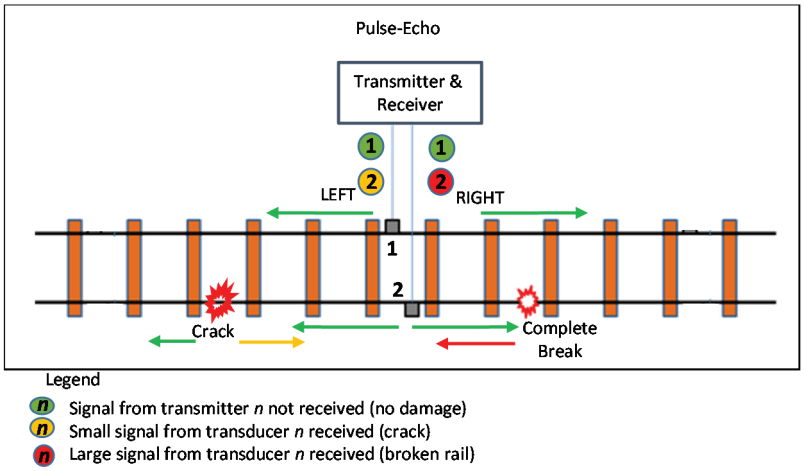

Fig. 1. A diagram illustrating the operation of a pulse-echo transducer

GWU-based monitoring systems are complicated by the fact that many different propagating modes are simultaneously excited by an attached transducer. These modes each propagate at different speeds and are generally dispersive. These complex propagation characteristics are usually presented in the form of dispersion curves and are required when performing signal processing in order to detect and locate defects. The semi-analytical finite element (SAFE) method has become a popular method for efficiently computing dispersion curves of elastic waveguides.
The dispersion curves of a rail are dependent on material properties as well as the rail geometry, neither of which are known to a sufficient degree of accuracy. The rail geometry in particular changes over time due to wear and regular maintenance operations which include rail grinding of the crown (to restore the profile and prevent shelling). It is therefore useful if the dispersion curves of the rail or rail properties can be estimated from measured signals obtained by the monitoring system.

The material and geometric parameters are implicit in the computation of the dispersion curves, and therefore in order to infer these properties from dispersion curves, an inverse problem needs to be solved using an iterative approach. During the later solution of the inverse problem it will be advantageous if the forward problem can be solved efficiently. In this study the forward problem of computing dispersion curves using SAFE is investigated for efficient and accurate computation of dispersion curves. A mesh convergence study is performed to determine a suitable discretisation such that results are not mesh dependant. Modes which propagate long distance in rail are identified and a procedure to track these modes in the frequency domain is presented. Finally, in order to efficiently compute the dispersion curves, a model reduction method (Guyan reduction) is presented.

Solution of the inverse problem will also be simplified if the number of rail parameters to be estimated can be reduced. These parameters include geometric parameters and material properties. Geometric parameters which describe the head wear are established. The geometry of the rail is then described using these parameters and an automated re-meshing strategy using radial basis functions is presented. Material properties of the SAFE formulation are written in terms of the ratio of elastic modulus and density (longitudinal speed of sound). It is shown that a simple scaling of the dispersion curves is possible when considering materials with a different elastic modulus-density ratio, but the same Poisson's ratio.

In section 2 experimental measurements are presented and analysed to identify the modes of propagation that need to be modelled. Section 3 provides a brief description of the SAFE formulation together with a convergence study to determine a suitable mesh discretization for performing the SAFE analyses. The method used to track different mode shapes computed at different frequencies and from different SAFE models is also presented. The minimum set of geometric parameters required to present rail profile change due to wear and grinding are identified in section 4, and an adaptive meshing technique is developed. Non-dimensional analysis is used to determine the minimum set of material properties that are required for analysis in section 4. Conclusions are listed in section 5.

2. Experimental setup and mode identification

Pulse-echo measurements were conducted on a heavy duty rail line. A tone burst (waveform) is transmitted using a transducer that is attached to the head of the UIC60 rail and mainly excites modes with energy concentrated in the head of the rail. Propagating modes are scattered at welds and may therefore be reflected as the incident mode or as a different mode [2]. Modes which propagate to the weld as a certain mode but return to the transducer as a different mode will be referred to as coupled modes.

The pulse-echo experimental setup is illustrated in Fig. 2(a). The experimental measurements employ a single transducer to both excite the propagating waves and to sense the reflections. Each mode propagates a round trip distance to a weld and back at a group velocity that is assumed constant along the rail. A measured time signal is shown in Fig. 2(b), with reflections from welds visible at approximately 50 ms and from a different weld again at around 100 ms.

A Short-Time Fourier Transform (STFT) [3] is performed on the measured signal to produce the spectrogram shown in Fig. 2(c). The spectrogram, which presents measurements in the time-frequency domain, provides a convenient way to compare SAFE and experimental data. The spectrogram in Fig. 2(c) has artefacts representing the frequency-dependent arrival times of the different propagating modes as they reflect from welds in the rail. The arrival times are frequency dependent due to the frequency dependent nature of the group velocity curves, see Fig. 4(b). Fig. 2(c) highlights time-of-arrival curves associated with one specific weld containing two uncoupled modes (which propagate to the weld, reflect and return as the same mode) and one coupled mode. The mode shapes of the propagating modes associated with these three time of arrival curves are depicted in Fig. 2(d).

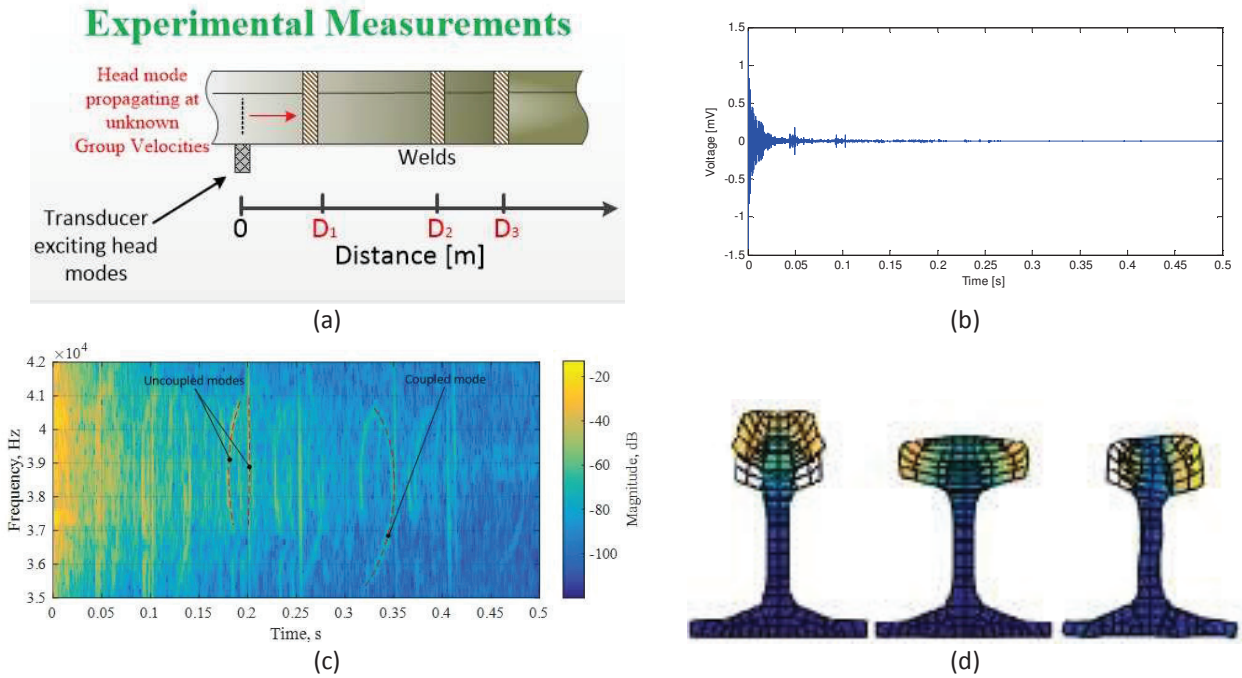

Fig. 2. Experimental measurements and identification of modes, (a) illustration of the GWU pulse-echo experimental setup (b) time signal measurements conducted on a UIC60 rail (c) STFT of the time signal measurement showing coupled and uncoupled modes (d) mode shapes that are expected to propagate in the rail.

3. SAFE analysis

The SAFE method has become popular for analysing guided wave propagation [4]. The problem under consideration is the analysis of the dispersion characteristics of an elastic isotropic waveguide of arbitrary but constant cross-section and infinite length, in a vacuum, as shown in Fig. 3. Wave propagation is along the *z*-direction, with constant cross-section in the *x – y* plane.

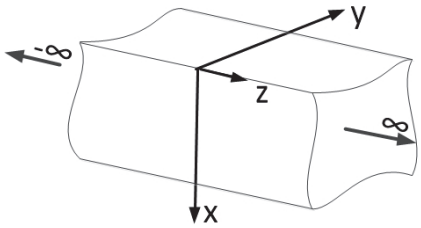

Fig. 3. Schematic of an infinite waveguide with arbitrary but constant cross-section.

3.1. SAFE formulation

In the SAFE formulation finite element discretization is performed only over the cross-section of the waveguide while the displacement distribution along the waveguide is described analytically. Spatial displacement amplitudes of the waveguide u_x, u_y and u_z respectively in the x, y and z-direction are defined as proposed by Gavric [5]. This formulation assumes a harmonic solution in the propagation direction, z

$$\begin{aligned} u_x(x,y,z,t) &= u_x(x,y)e^{i(\kappa z-\omega t)} \\ u_y(x,y,z,t) &= u_y(x,y)e^{i(\kappa z-\omega t)} \\ u_z(x,y,z,t) &= u_z(x,y,z,t)e^{i\left(\kappa z-\omega t-\frac{\pi}{2}\right)} = -iu_z(x,y,z,t)e^{i(\kappa z-\omega t)} \end{aligned} \tag{1}$$

where, κ and ω are the wavenumber and frequency respectively, and i is the imaginary unit. The phase correction in the *z*-displacement interpolation ensures that symmetric stiffness and mass matrices are obtained.

After application of the method, see for example [5], and assembly of global matrices the following systems of equations are obtained:

$$[\mathbf{K}_1 + i\kappa\mathbf{K}_2 + \kappa^2\mathbf{K}_3 - \omega^2\mathbf{M}]_M\mathbf{Q} = \mathbf{0} \tag{2}$$

where $\mathbf{K}_i$ represents the stiffness matrix *i*, the mass matrix is given by $\mathbf{M}$ and $\mathbf{Q}$ denotes the assembled displacements. *M* represents the number of system degrees of freedom. Note that unlike the convensional finite element method, there are three stiffness matrices; one independent of κ, one proportional to κ and the other proportional to κ^2. The eigenvalue problem in (2) can be solved by fixing κ and solving ω^2. Alternatively if the solution at a particular frequency is required, the system of equations is arranged such that

$$[\mathbf{A} - \kappa\mathbf{B}]_{2M}\overline{\mathbf{Q}} = \mathbf{0} \tag{3}$$

where

$$\mathbf{A} = \begin{bmatrix} \mathbf{K}_1 - \omega^2\mathbf{M} & \mathbf{O} \\ \mathbf{O} & -\mathbf{K}_3 \end{bmatrix}, \mathbf{B} = \begin{bmatrix} -i\mathbf{K}_2 & -\mathbf{K}_3 \\ -\mathbf{K}_3 & \mathbf{O} \end{bmatrix}, \overline{\mathbf{Q}} = \begin{bmatrix} \mathbf{Q} \\ \kappa\mathbf{Q} \end{bmatrix}$$

and $\mathbf{O}$ represents a zero matrix of size $M \times M$. Solution equation (3) results in $2M$ eigenvalue outputs of M forward and M backward pairs of eigenvalues. Computed eigenvalues may be real, complex or imaginary. Complex and imaginary eigenvalues represent evanescent modes, whereas real eigenvalue represent propagating modes at selected frequencies. In this study we are only interested in propagating modes.

Bartoli [6] shows how the group velocity, c_g, of propagating modes can be computed using equation (2),

$$c_g = \frac{\partial \omega}{\partial \kappa} = \frac{\mathbf{Q}(i\mathbf{K}_2 + 2\kappa\mathbf{K}_3)\mathbf{Q}}{2\omega\mathbf{QMQ}}. \quad (4)$$

3.2. SAFE mode tracking

In order to compare the computed SAFE results with the experimentally measured spectrograms, a method is required to convert the discrete wavenumber-frequency and associated group velocity-frequency points computed using SAFE to continuous curves. Loveday et al. [7] have shown that wavenumber-frequency curves of symmetric and antisymmetric families of modes do not cross within a given family, and that mode shapes can swap in so-called repulsion regions. This mode shape swapping can result in difficulties if the mode numbering order changes with material or geometric properties. For this study it is therefore appropriate to apply a tracking method based on mode shape rather than mode number since the three mode shapes of interest are known. The Modal Assurance Criterion (MAC) [8], which performs correlation of mode shapes, is implemented to track head modes for all calculated dispersion points at selected frequencies. The formula for MAC proposed by Ting et al [8] is given as:

$$MAC(\Phi_{Ai}, \Phi_{Xj}) = \frac{\left|\{\Phi_A\}_i^T \{\Phi_X\}_j\right|^2}{\{\Phi_A\}_i^T \{\Phi_A\}_i \{\Phi_X\}_j^T \{\Phi_X\}_j} \quad (5)$$

where Φ_{Ai} and Φ_{Xj} are the i and j eigenvectors of the reference and tracked mode shapes.

A correlation, ranging from 0 to 1, is computed using the reference and tracked mode shapes. Values closer to 0 indicate that mode shapes are not similar while values closer to 1 indicate close similarity between the compared mode shapes. To set up the process of extracting mode shapes from calculated dispersion points, three groups of corresponding head mode shapes (reference mode shapes) were created for the unworn UIC60 rail by manually extracting head mode shapes in the frequency range of 34-44 kHz at twenty equally spaced frequency interval points. Examples of the frequency-dependent mode shapes, for the 3 modes which have been experimentally measured, are depicted in Fig. 4. All mode shapes from the reference group (Group 1, 2 and 3) are correlated with mode shapes computed using new SAFE models (tracked mode shapes). This is conducted with the assumption that a mode shape that corresponds with each group propagates at the frequency of interest and can therefore be extracted. The tracked mode shape with the highest sum of correlation values for each group is regarded as the mode shape for that group. Fig. 4(b) shows the group velocity dispersion curves extracted at each frequency point using this procedure. Inspection of extracted dispersion points has shown that correct modes were extracted to form dispersion curves.

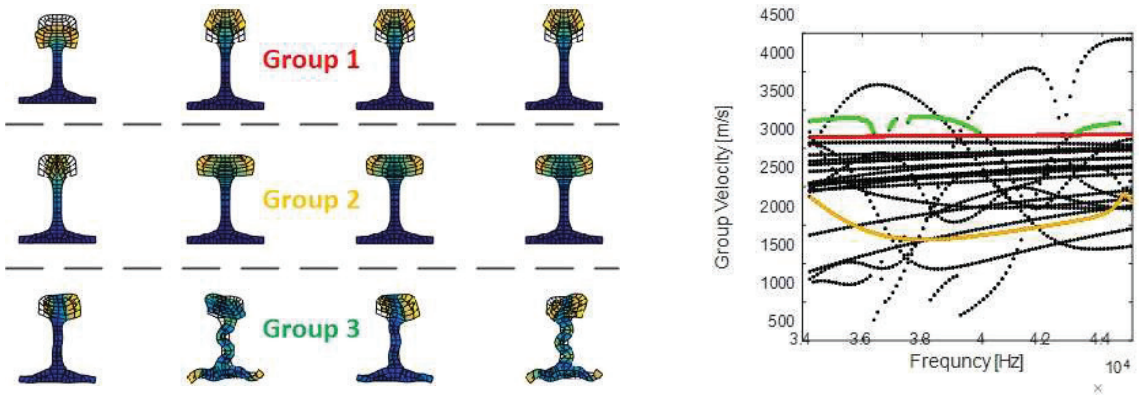

(a) (b)

Fig. 4. (a) Mode shape groups used for tracking computed SAFE models (b) Plots of dispersion solution computed using a SAFE model of the pristine rail profile and superimposed plots of tracked dispersion curves (highlighted in green, red and yellow).

3.3. Analysis of SAFE method convergence

The plots in Fig. 5 show convergence of the group velocity solutions at $40\ kHz$ for four different element types.

Linear and quadratic triangular elements are denoted T3 and T6 respectively with 4- and 8-noded quadrilateral elements are labelled Q4 and Q8, respectively. Mesh convergence using the group velocity for the three modes identified in Fig. 2(d) is considered. Unlike the convergence behaviour for regular shaped waveguides which exhibit different convergence rates for linear and quadratic elements [9], first-order convergence is observed for all element types in Fig. 5. This is as a result of the complex shape of the rail profile. Fig. 5 suggests that the Q8 element achieves the best accuracy for a given number of system degrees of freedom. Furthermore, since the Q8 mesh with 1005 nodes achieves an error of less than 1% for each of the modes of propagation analysed, this mesh is considered sufficiently accurate and will be used in the remainder of the study.

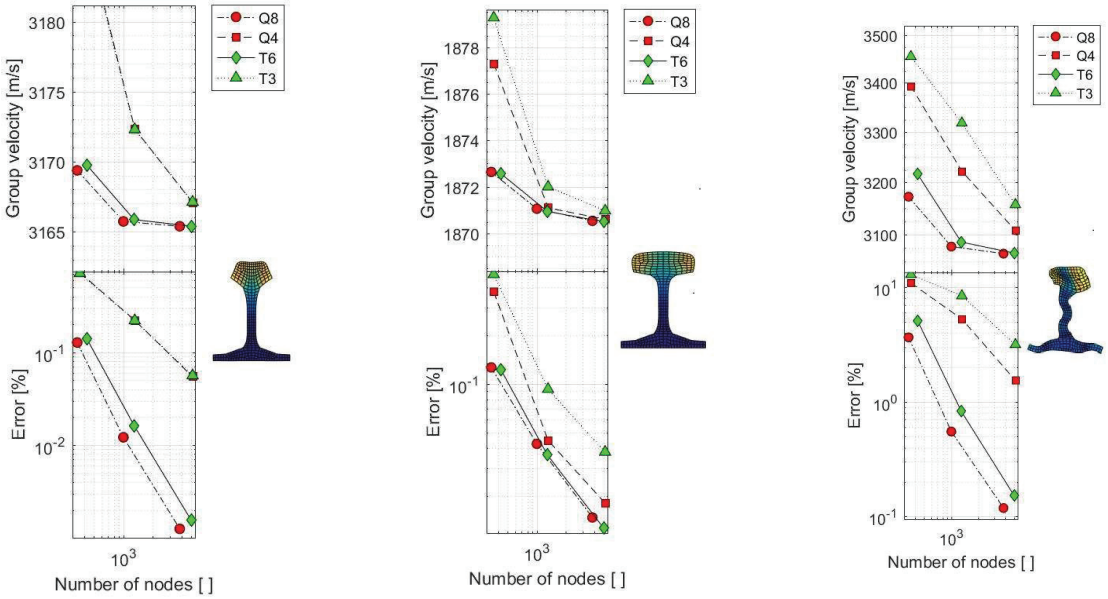

Fig. 5. Convergence plots of the group velocity for the modes that were studied, (a) Group 1 mode shape (b) Group 2 mode shape (c) Group 3 mode shape

3.4. Solution of the SAFE eigenvalue problem using Guyan reduction

Matrix condensation could be used to improve the efficiency of obtaining eigenvalue solutions from SAFE models. In matrix condensation, global mesh coordinates are separated into master and slave coordinates of the original mass and stiffness matrices to reduce the size of the matrices. Various formulations and a comparison of matrix condensation techniques are discussed in [10].

Guyan's reduction technique is appropriate for the nature of the mode shapes considered for this study [10]. The modes which propagate long distance in the rail have deformation energy concentrated in the head of the rail. We therefore investigate condensation of the degrees of freedom in the web and foot of the rail. Guyan's reduction procedure is applied to the equation of motion in (2) for the original rail eigenvalue problem with wavenumber (κ) specified. In this case (2) reduces to

$$[\mathbf{K} - \omega^2\mathbf{M}]\mathbf{Q} = \mathbf{0}. \tag{6}$$

The mass and stiffness matrices are partitioned into master and slave degrees of freedom as

$$\left[\begin{bmatrix}\mathbf{K}_{mm} & \mathbf{K}_{ms}\\ \mathbf{K}_{sm} & \mathbf{K}_{ss}\end{bmatrix} - \omega^2\begin{bmatrix}\mathbf{M}_{mm} & \mathbf{M}_{ms}\\ \mathbf{M}_{sm} & \mathbf{M}_{ss}\end{bmatrix}\right]\begin{Bmatrix}\mathbf{Q}_m\\ \mathbf{Q}_s\end{Bmatrix} = \mathbf{0} \tag{7}$$

where subscripts m and s represent selected master and slave coordinates of the original mesh. After performing Guyan's reduction method on equation (2), we can solve the reduced eigenvalue problem in equation (8).

$$[\overline{\mathbf{K}}_{mm} - \omega^2 \overline{\mathbf{M}}_{mm}]\mathbf{Q}_m = \mathbf{0} \quad (8)$$

where $\overline{\mathbf{K}}_{mm}$ and $\overline{\mathbf{M}}_{mm}$ are the condensed/reduced stiffness and mass matrices. In order to test the accuracy of this method for the UIC-60 rail, master coordinates associated with nodes in the head and part of the web from a height of $95\ mm$ above the base of the rail, as depicted in Fig. 6, were retained and results compared to a full model for all head modes propagating in the frequency range of 34 to $44\ kHz$. This height was selected by inspection of the concentration of energy at $39\ kHz$ for the three mode shapes that are considered, as shown in Fig. 6(b).

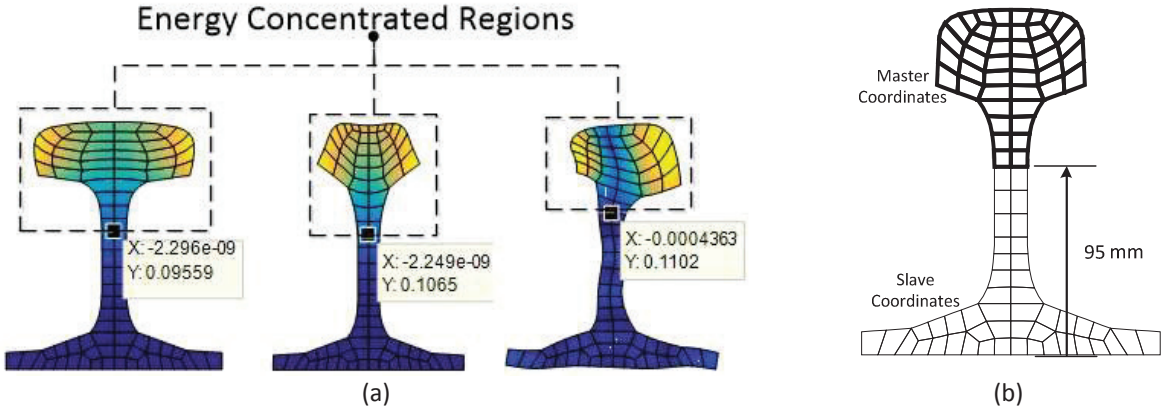

Fig. 6. Analysis of mode shapes for Guyan reduction, (a) Energy concentration of the investigated mode shapes at a frequency of $39\ kHz$ (b) Selected height for separating master and slave coordinates.

Wavenumber-frequency dispersion points of the reduced model employing Guyan reduction, are superimposed on those computed using the full model for a UIC60 rail profile in Fig. 7. The figure also shows the percentage error of the reduced model relative to the full mode at the computed wavenumbers. In the figure, $\omega_i^{SAFE}(\kappa)$ and $\omega_i^{Guyan}(\kappa)$ represent the frequency solutions computed using the SAFE full model and reduced model respectively, where i represents the different groups of mode shapes illustrated in Fig. 4.

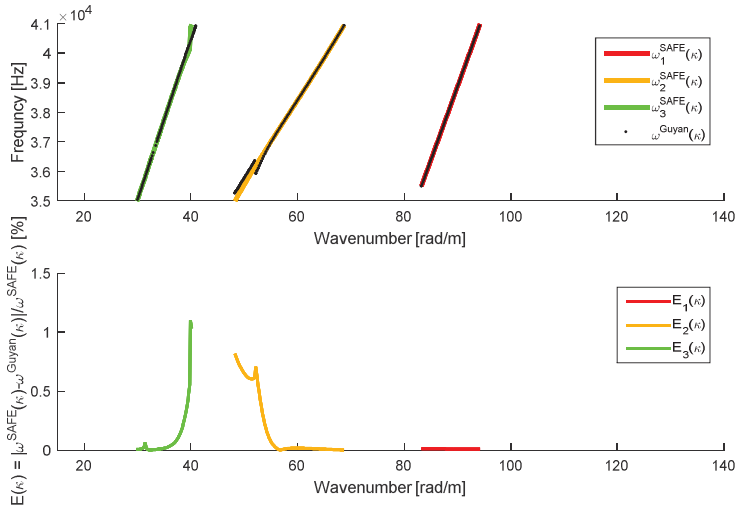

Fig. 7. Comparison of frequency-wavenumber solutions (for the three mode shape groups) computed using a full SAFE model and the same model reduced using Guyan's reduction method, and plots of the frequency error for wavenumber inputs.

The relatively small difference between the reduced and the full models depicted in Fig. 7 indicate that Guyan reduction is appropriate for computing the dispersion curves of modes with energy concentrated in the head of the rail in the specified frequency range. The largest discrepancies between the two models occur near mode repulsion points [7] since energy is not as concentrated in the rail head at these points, resulting in an inaccurate computation of the reduced model.

4. Parameterization of the UIC60 rail

In this section, a minimal set of parameters to fully describe the rail condition are described. Both geometric and material parameters are included since both affect the speed of wave propagation in the rail. The geometry of the rail is dependent on the amount of wear and maintenance that the rail has been exposed to, while material properties are dependent on environmental conditions (with the modulus of elasticity for example being temperature dependant).
In this section, first the geometric parameters to describe the rail geometry are proposed, together with a method to update the SAFE mesh based on these parameters. This is followed by a presentation of a reduced set of material parameters as a result of combining (or non-dimensionalising) elastic modulus, density and frequency.

4.1. Rail geometric parameterisation

The rail geometry changes over time due to routine maintenance operations, such as rail grinding, and wear. Wear is dependent on factors such as the type of rail profile, curvature of the track, wheel profile and loading [11]–[14]. Various combinations of dimensions were investigated for representing realistic worn rail profiles. In order to describe the possible rail head geometries encountered in practice, it was found that at least three parameters are required. These three parameters are shown in Fig. 8(a) for the UIC60 rail.

Geometric parameters X_1, X_2 and X_3 describe the reduction in the head height, increased interior radius and a sharper exterior radius, respectively. In order to demonstrate that the design parameterization depicted in Fig. 8 is capable of representing the measured rail profile, the geometry generated using the parameters in Fig. 8(a) is overlaid on the measured profile in Fig. 8(c). Good agreement is observed between the generated rail profile and the measured profile. The amount of wear in this case is evident by comparison with an unworn rail profile; see Fig. 8(b).

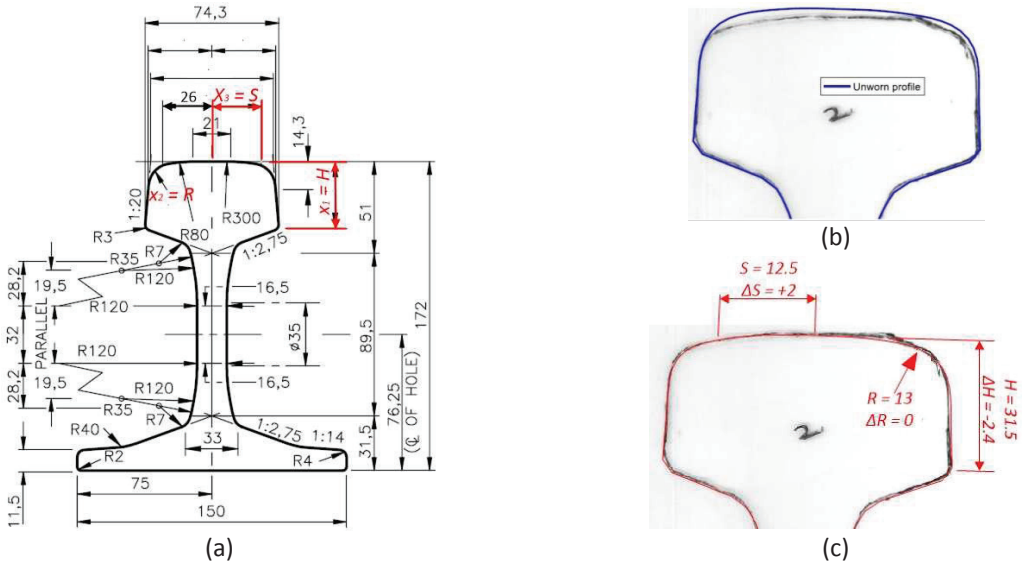

Fig. 8. Profiles of the UIC60 rail, (a) pristine profile of the UIC60 rail showing parameters used to simulate wear (b) overlay of the unworn profile on the worn profile measured in the field (c) overlay of simulated profile for estimate of the worn profile.

4.2. Mesh adaptation

In order to perform SAFE analyses of worn rails, the mesh of the unworn rail (which is created manually) needs to be adapted based on the geometries resulting from the rail boundary parameterisation. The process employed in this study for meshing worn profiles of the UIC60 rail is illustrated in Fig. 9. First nodes on the boundary are moved to coincide with the boundary parameterisation. Internal nodal positions are thereafter updated based on the position of the boundary nodes using Radial basis functions (RBFs) [15]. The RBF is designed such that re-meshing is conducted without external user input and minimising mesh distortion.

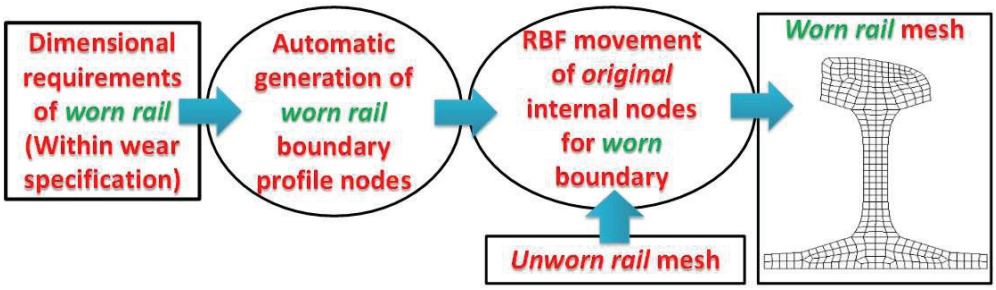

Fig. 9. Illustration of the process used to adapt meshes using RBFs.

Three meshes depicting an unworn UIC60 rail profile, worn UIC60 profile without mesh movement and one with mesh movement, are shown in Fig. 10. The meshes in Fig. 10(c)–(d) were modified based on the "new profile" shown in Fig. 10(a). The three meshes are comprised of eight-noded quadrilateral elements.

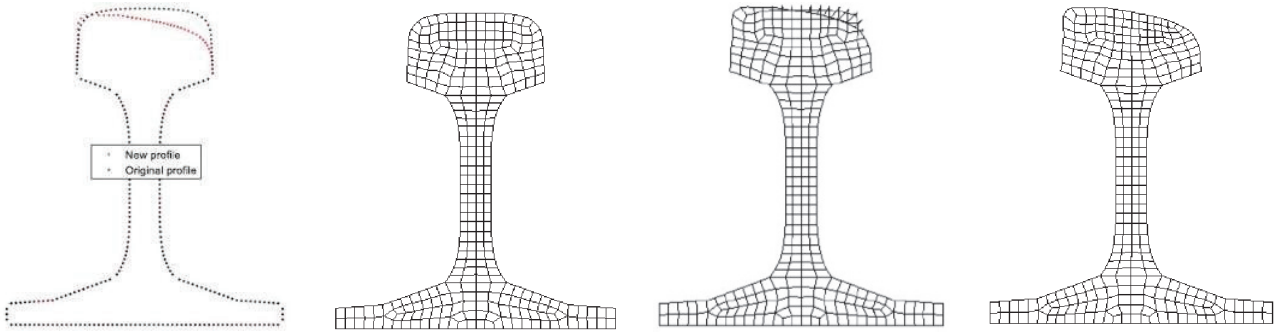

Fig. 10. (a) Two profiles, the original rail profile and a simulation of a worn/new profile. (b) Original mesh of the rail (c) Worn profile without application mesh movement (d) Worn profile with application of mesh movement

The meshes in Fig. 10 show that distortion of the mesh boundary elements is avoided when mesh movement is employed. Close observation of the deformed mesh with mesh movement in Fig. 10(d) shows that the nodal displacement interpolations have greater displacements near the deformed boundary. The worn rail boundary mesh without mesh movement in Fig. 10(d) clearly shows that the mesh is distorted when the head boundary is displaced downwards, with some elements becoming inverted.

4.3. Material parameterization

The material properties of the rail can be described by the steel elastic modulus, E, Poisson's ratio, ν, and the material density, ρ. These material properties are not known to an acceptable accuracy, and are dependent on environmental conditions (with the elastic modulus in particular being temperature dependant).

It can be shown that the constants E and ρ can be factored out of the stiffness and mass matrices, respectively as follows:

$$\mathbf{K}_1 = E\sum_{k=1}^{n}\overline{\mathbf{k}}_1^{(e)}, \mathbf{K}_2 = E\sum_{k=1}^{n}\overline{\mathbf{k}}_2^{(e)}, \mathbf{K}_3 = E\sum_{k=1}^{n}\overline{\mathbf{k}}_3^{(e)} \quad \mathbf{M} = \rho\sum_{k=1}^{n}\overline{\mathbf{m}}^{(e)} \tag{9}$$

Using these factored global stiffness and mass matrices, the discretized equation of motion can be re-written as

$$[\overline{\mathbf{K}}_1 + i\kappa\overline{\mathbf{K}}_2 + \kappa^2\overline{\mathbf{K}}_3 - \frac{\rho}{E}\omega^2\overline{\mathbf{M}}]_M\mathbf{Q} = \mathbf{0}. \tag{10}$$

Equation (10) shows that for our application, the density and elastic modulus can be combined as a single input parameter for the SAFE analysis. The relationship between ρ and E in equation (10) can be substituted with the equivalent longitudinal speed of sound, c, where $c^2 = E/\rho$. By combining these two material parameters, the number of unique parameters describing the wave propagation is reduced by one. The discretized equation of motion is then re-written as:

$$[\overline{\mathbf{K}}_1 + i\kappa\overline{\mathbf{K}}_2 + \kappa^2\overline{\mathbf{K}}_3 - \frac{\omega^2}{c^2}\overline{\mathbf{M}}]_M\mathbf{Q} = \mathbf{0}. \tag{11}$$

As demonstrated in Section 3.1, equation (2) can be solved by either selecting the wavenumber, κ, and solving for the frequency, ω, or by selecting a frequency and solving for the wavenumber. In the latter case where ω is specified, equation (11) shows that the frequency and the speed of sound, c, may again be combined to a single parameter, β, which is given by the ratio of the input frequency and speed of sound

$$\beta = \frac{\omega}{c}. \tag{12}$$

The discretized equation of motion in equation (2) can therefore be written as:

$$[\overline{\mathbf{K}}_1 + i\kappa\overline{\mathbf{K}}_2 + \kappa^2\overline{\mathbf{K}}_3 - \beta^2\overline{\mathbf{M}}]_M\mathbf{Q} = \mathbf{0}. \tag{13}$$

The group velocity relation in equation (4) can similarly be rewritten as

$$c_g \quad = c\frac{\mathbf{Q}^T(\overline{\mathbf{K}}_2 + 2\kappa\overline{\mathbf{K}}_3)\mathbf{Q}}{2\beta\mathbf{Q}^T\overline{\mathbf{M}}\mathbf{Q}}. \tag{14}$$

The important implication of equations (13) and (14) is that if $\beta = \omega/c$ is solved over a wide enough range, results for different material properties (with different E and ρ) can be generated without resolving the eigenvalue problem. Thus, these results (dispersion curves for different E and ρ or c) can be determined by scaling the already computed dispersion curves. This is true since β contains both ω and material parameters, $c^2 = E/\rho$.

To verify this observation, wavenumber-frequency and group velocity-frequency dispersion curves are solved by selecting β and then scaled such that the results represent materials with two different speeds of sound. The same dispersion curves are solved by solving equations (13) twice with the appropriate properties. Dispersion plots of the slow head mode solved using these two solution approaches are shown in Fig. 11. Solutions are depicted for speeds of sound, $c = 5000$ m/s and $c = 5050$ m/s for a frequency range of 36 to 40 kHz.

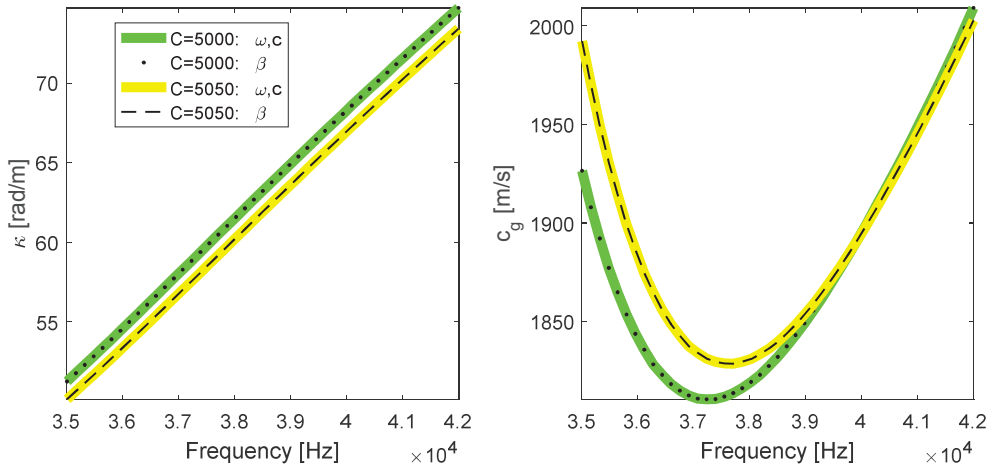

Fig. 11. Comparison of dispersion curves computed using two methods. For the one method dispersion curves are computed using β. The other method used different properties of c to solve for the problem twice

Fig. 11 illustrates that the same dispersion curves are computed by solving for $\beta = \omega/c$ and scaling the outputs to reflect the correct material properties using $c^2 = E/\rho$, or by specifying two different materials and solving the eigenvalue problems separately over the range of frequencies. In order to facilitate this scaling however, for a fixed range of ω, $\beta = \omega/c$ dispersion curves must be computed over a slightly larger range to allow wider determination of material properties, $c^2 = E/\rho$. Fig. 11 also demonstrates that changing the longitudinal speed of sound, c, results in a simple scaling of the wavenumber over frequency, while a more complex scaling results for the group velocity, with a shift in both group velocity and frequency as a result of β appearing in the expression for group velocity, c_g.
Using the proposed method, only two material properties need to be selected (c, ν) instead of three (E, ρ, ν). Furthermore, in addition to this saving of computation time, the dispersion curves for each combination of (c, ν) only needs to be solved once, while other values of c can be determined by scaling β. It should be noted that β is not dependent on Poisson's ratio, ν, and therefore the eigenvalue problem needs to be re-solved for each ν value.

5. Conclusions

Experimental results showed that three propagating modes could be detected in the field, after reflecting from welds in the rail. The focus of the analysis was therefore on these three modes. Modal Assurance Criteria (MAC) was adopted to track the mode shapes computed using the SAFE method. This allowed convenient tracking of mode shapes that were computed using different material and geometric properties of the rail.

The convergence of the group velocity with mesh refinement was studied for different elements and the Q8 element was found to be the most efficient and was used in the rest of the study. It was demonstrated that Guyan reduction can be employed to reduce the size of the eigenvalue problem under some circumstances. This method was demonstrated by solving the dispersion curves for the three modes which were found to propagate long distance in rails.

A set of parameters which can be used to construct an accurate SAFE model of a worn rail were determined. These parameters describe both the geometry and the material properties of the rail, and were used to compute the dispersion curves, which describe the wave propagation characteristics of the rail.

It was found that the wear and grinding of the rail head can be adequately represented by changing only three geometric parameters. An adaptive mesh model for simulating material removal (wear and grinding) of the rail head was developed using parametric equations and a mesh movement algorithm using radial basis functions was employed to generate meshes of the rail from the parameterized geometry. The model allows efficient modification of the geometry and mesh of the rail using parameters, instead of manually producing a new rail profile and re-meshing.

It was shown that for an isotropic elastic medium, the elastic modulus and density can be combined and considered as a single variable, the longitudinal speed of sound in the medium given by $c = \sqrt{E/\rho}$. The efficiency of the SAFE computations were further improved by solving the eigenvalue problem in terms of a ratio of the frequency and longitudinal speed of sound through the introduction of the parameter $\beta = \omega/c$. It was shown that solving the eigenvalue problem in this way, only a single set of dispersion curves need to be calculated using SAFE for each Poisson's ratio. The dispersion curves for materials with the same Poisson's ratio but different values of c can be generated using a simple scaling without having to re-solve the eigenvalue problem.

The efficient SAFE model with minimal input parameters will be used in future to investigate the inverse problem of identifying the input parameters from experimental measurements of the group velocities.

Acknowledgements

The authors would like to thank the CSIR for opportunity to conduct this work.

References

[1] F. A. Burger and PW Loveday, “Ultrasonic broken rail detector and rail condition monitor technology,” in

Proceedings of the 11th International Heavy Haul Association Conference (IHHA 2017), 2017, pp. 275–280.
[2] C. S. Long and P. W. Loveday, "Prediction of guided wave scattering by defects in rails using numerical modelling," in *AIP Conference Proceedings 1581*, 2014, p. 240.
[3] P. Welch, "The use of Fast Fourier Transform for the estimation of Power Spectra: A method based on time averaging over short, modified periodograms," *IEEE Trans. Audio Electroacoust.*, vol. au-15, no. 2, pp. 70–73, 1967.
[4] J. L. Rose, "Ultrasonic guided waves in solid media," in *Ultrasonic Guided Waves in Solid Media*, 1st ed., vol. 9781107048, New York NY: Cambridge University Press, 2014, pp. 135–153.
[5] L. Gavric, "Computation of propagative waves," *J. Sound Vib.*, vol. 185, no. 3, pp. 531–543, 1995.
[6] I. Bartoli, A. Marzani, F. Lanza di Scalea, and E. Viola, "Modeling wave propagation in damped waveguides of arbitrary cross-section," *J. Sound Vib.*, vol. 295, no. 3–5, pp. 685–707, 2006.
[7] P. W. Loveday, C. S. Long, and D. A. Ramatlo, "Mode repulsion of ultrasonic guided waves in rails," *Ultrasonics*, vol. 84, pp. 341–349, 2018.
[8] T. Ting, T. L. C. Chen, and W. Twomey, "Correlating mode shapes based on the modal assurance criterion," *Finite Elem. Anal. Des.*, vol. 14, no. 4, pp. 353–360, 1993.
[9] E. V. Andhavarapu, P. W. Loveday, and C. S. Long, "Accuracy of Semi-Analytical Finite Elements for modeling wave propagation in rails," in *Seventh South African Conference on Computational and Applied Mechanics*, 2010, no. January, pp. 10–13.
[10] J. Wijker, "Mechanical Vibrations in Spacecraft Design," in *Mechanical Vibrations in Spacecraft Design*, 1st ed., Berlin: Springer, 2004, pp. 343–367.
[11] C. Chongyi, W. Chengguo, and J. Ying, "Study on numerical method to predict wheel/rail profile evolution due to wear," *Wear*, vol. 269, no. 3–4, pp. 167–173, 2010.
[12] J. Gerlici and T. Lack, "Railway wheel and rail head profiles development based on the geometric characteristics shapes," *Wear*, vol. 271, no. 1–2, pp. 246–258, 2011.
[13] P. Wang, J. Xu, K. Xie, and R. Chen, "Numerical simulation of rail profiles evolution in the switch panel of a railway turnout," *Wear*, vol. 366–367, pp. 105–115, 2016.
[14] M. Ignesti, M. Malvezzi, L. Marini, E. Meli, and A. Rindi, "Development of a wear model for the prediction of wheel and rail profile evolution in railway systems," *Wear*, vol. 284–285, pp. 1–17, 2012.
[15] A. De Boer, M. S. Van Der Schoot, and H. Bijl, "New Method for Mesh Moving Based on Radial," in *European Conference on Computational Fluid Dynamics ECCOMAS*, 2006, pp. 1–16.